JASA ARTICLE

Application of damped cylindrical spreading to assess range to injury threshold for fishes from impact pile driving[a)]

Michael A. Ainslie,[1,b)] Michele B. Halvorsen,[2,c)] Roel A. J. Müller,[3] and Tristan Lippert[4,d)]

[1]*JASCO Applied Sciences (Deutschland) GmbH, Mergenthaler Allee 15-21, 65760 Eschborn, Hesse, Germany*

[2]*CSA Ocean Sciences Inc., 8502 Southwest Kansas Avenue, Stuart, Florida 34997, USA*

[3] *TNO Acoustics and Sonar, Oude Waalsdorperweg 63, 2597 AK Den Haag, the Netherlands*

[4]*Technische Universität Hamburg, 21071 Hamburg, Germany*

ABSTRACT:

Environmental risk assessment for impact pile driving requires characterization of the radiated sound field. Damped cylindrical spreading (DCS) describes propagation of the acoustic Mach cone generated by striking a pile and predicts sound exposure level (L_E) versus range. For known water depth and sediment properties, DCS permits extrapolation from a measurement at a known range. Impact assessment criteria typically involve zero-to-peak sound pressure level ($L_{p,\mathrm{pk}}$), root-mean-square sound pressure level ($L_{p,\mathrm{rms}}$), and cumulative sound exposure level ($L_{E,\mathrm{cum}}$). To facilitate predictions using DCS, $L_{p,\mathrm{pk}}$ and $L_{p,\mathrm{rms}}$ were estimated from L_E using empirical regressions. Using a wind farm construction scenario in the North Sea, DCS was applied to estimate ranges to recommended thresholds in fishes. For 3500 hammer strikes, the estimated $L_{E,\mathrm{cum}}$ impact ranges for mortal and recoverable injury were up to 1.8 and 3.1 km, respectively. Applying a 10 dB noise abatement measure, these distances reduced to 0.29 km for mortal injury and 0.65 km for recoverable injury. An underlying detail that produces unstable results is the averaging time for calculating $L_{p,\mathrm{rms}}$, which by convention is equal to the 90%-energy signal duration. A stable alternative is proposed for this quantity based on the effective signal duration.

 https://doi.org/10.1121/10.0001443

(Received 24 December 2019; revised 15 May 2020; accepted 31 May 2020; published online 8 July 2020)

[Editor: Arthur N. Popper] Pages: 108–121

I. INTRODUCTION

Construction of offshore wind farms extensively uses impact pile driving to install monopile, tripod, and jacket foundations for each wind turbine. In Germany, measurements of sound exposure level (L_E) and zero-to-peak sound pressure level ($L_{p,\mathrm{pk}}$) were made during the construction of the Borkum Riffgrund 1 (BR1) wind farm. Measured noise levels reported at a range of 28 m from a 6 m diameter monopile were 190–193 dB re 1 μPa^2 s (single strike sound exposure level, $L_{E,\mathrm{ss}}$) and 218–221 dB re 1 μPa^2 ($L_{p,\mathrm{pk}}$), depending on the hydrophone depth (ITAP, 2015a). For otherwise fixed conditions, the larger the pile diameter, the higher the hammer energy needed to drive the pile into the sediment. Values of $L_{E,\mathrm{ss}}$ and $L_{p,\mathrm{pk}}$ increase with increasing pile diameter and hammer energy, due to the increase in the energy radiated from the surface of the pile wall (Heitmann, 2016). Risks to aquatic life associated with impulsive signals generated by pile driving include hearing threshold shift (Finneran *et al.*, 2000; Finneran *et al.*, 2002; Finneran *et al.*, 2003; Finneran *et al.*, 2015; Lucke *et al.*, 2009; Finneran, 2015; Kastelein *et al.*, 2015; Kastelein *et al.*, 2016; Kastelein *et al.*, 2017; Kastelein *et al.*, 2018), tissue injury (Halvorsen *et al.*, 2011, 2012b; Halvorsen *et al.*, 2012a; Casper *et al.*, 2012; Casper *et al.*, 2013a, Casper *et al.*, 2013b; Casper *et al.*, 2017), and avoidance (Tougaard *et al.*, 2009; Dähne *et al.*, 2013).

Reinhall and Dahl (2011) showed that the sound radiated close to the pile was in the form of a Mach cone traveling at an angle of approximately 17° from the horizontal (73° incidence angle). Propagation of the Mach cone away from the pile leads to a region of damped cylindrical spreading (DCS) of the acoustic signal (Zampolli *et al.*, 2013; Ainslie *et al.*, 2014; Lippert *et al.*, 2018; Martin and Barclay, 2019). With a single measurement of L_E at a known range, the DCS model (Lippert *et al.*, 2018) provides a means for predicting L_E as a function of range from the pile when the water depth and sediment grain size are uniform (independent of range) and known.

Environmental risk assessment typically requires knowledge of $L_{E,\mathrm{cum}}$, $L_{p,\mathrm{pk}}$ (Popper *et al.*, 2014; Southall *et al.*, 2019) and root-mean-square (rms) sound pressure level ($L_{p,\mathrm{rms}}$) (Southall *et al.*, 2007; Scholik-Schlomer, 2015; GARFO, 2016).

For this study, the DCS method was expanded to estimate $L_{p,\mathrm{pk}}$ and $L_{p,\mathrm{rms}}$ (given L_E) using the regression method

[a)]This paper is part of a special issue on The Effects of Noise on Aquatic Life.

[b)]Electronic mail: michael.ainslie@jasco.com, ORCID: 0000-0002-0565-3559.

[c)]Current address: University of New Hampshire, School of Marine Science and Ocean Engineering, Durham, New Hampshire 03824, USA, ORCID: 0000-0002-2495-7574.

[d)]ORCID: 0000-0003-4764-1836.

https://doi.org/10.1121/10.0001443

used by Lippert *et al.* (2015). The DCS method is most accurate near the pile, where the acoustic metrics L_E and $L_{p,\mathrm{pk}}$ are calculated and compared with thresholds for injury to marine life. By contrast, $L_{p,\mathrm{rms}}$ is of interest mainly at long range from the pile, whereas DCS is applicable at short range (at least up to 5 km for this study; see Fig. 10), where the acoustic propagation is characterized by exponential decay associated with the Mach cone. The value of $L_{p,\mathrm{rms}}$ depends on the chosen averaging method, two of which were considered, based on the effective signal duration (Burdic, 1991) and the 90%-energy signal duration.

The basic DCS model (Lippert *et al.*, 2018) is summarized in Sec. II, followed by regressions for $L_{p,\mathrm{pk}}$ and $L_{p,\mathrm{rms}}$ (Sec. III), an investigation of possible measures of signal duration and associated mean-square sound pressure (Sec. IV), and validation of the DCS method (Sec. V). Application of DCS for analyzing the influence of pile-driving noise on fishes is discussed in Sec. VI, followed by conclusions in Sec. VII.

Acoustical terminology follows ISO (2017). International standard reference values (ISO, 2015) of $1\,\mu\mathrm{Pa}^2$ (L_p) and $1\,\mu\mathrm{Pa}^2\,\mathrm{s}$ (L_E) are used throughout. Following ISO (2017), this paper distinguishes between transmission loss (the difference between two $L_{p,\mathrm{rms}}$ or $L_{E,\mathrm{ss}}$ values) and propagation loss (the difference between source level and $L_{p,\mathrm{rms}}$).

II. OVERVIEW OF DCS

An impact-driven pile does not have a source level for two reasons. First, source level (ISO, 2017) is defined in terms of the sound radiated by a source into its far field, where the propagation is spherical. For an impact-driven pile, the extent of the source throughout the entire water column from seafloor to sea surface results in cylindrical spreading from the pile wall (Dahl *et al.*, 2012; Zampolli *et al.*, 2013). Thus there exists no region of spherical spreading, and therefore no far field. Second, the same definition of source level invokes the concept of "a hypothetical infinite uniform lossless medium of the same density and sound speed as the real medium at the location of the source," and therefore a source level is only defined if the source in question is in contact with a single uniform medium. The pile is in contact with a *layered* medium comprising water and sediment, with at least two different impedances, and therefore also does not meet this second criterion for the definition (i.e., existence) of a source level.

Because propagation loss is defined in terms of source level, if source level is undefined then so is propagation loss (Ainslie *et al.*, 2012; Heaney *et al.*, 2020). A more useful concept for a pile driver is the transmission loss (ΔL_{TL}), which is defined as the decrease in level from r_1 to r (ISO, 2017),

$$\Delta L_{\mathrm{TL}}(r;r_1) := L_E(r_1) - L_E(r), \tag{1}$$

where L_E is the sound exposure level integrated over one or more complete hammer strikes. For acoustic propagation in shallow water, it is common to parametrize ΔL_{TL} between two points at ranges r and r_1 from a source, in the form of

$$\Delta L_{\mathrm{TL}}(r;r_1) = 10\,\beta \log_{10}\frac{r}{r_1}\ \mathrm{dB}, \tag{2}$$

which, defining the transmission factor $F_{\mathrm{TL}} = 10^{-\Delta L_{\mathrm{TL}}/(10\,\mathrm{dB})}$, implies $F_{\mathrm{TL}}(r;r_1) = (r_1/r)^{\beta}$, with $\beta = 2$ and 1 corresponding to spherical and cylindrical spreading, respectively.

Close to the pile, the radiated sound field is dominated by a Mach cone (Reinhall and Dahl, 2011; Zampolli *et al.*, 2013), which carries a certain amount of energy from the pile. At range r, this energy is spread into area $2\Pi rH$, where H = water depth. Ignoring energy loss mechanisms, the energy flux density is inversely proportional to range, corresponding to cylindrical spreading ($\beta = 1$) (Dahl *et al.*, 2012). However, the attenuation due to multiple boundary reflections modifies this behavior, resulting in exponential decay, thus leading to DCS ($F_{\mathrm{TL}} \propto \mathrm{e}^{-2\alpha r}/r$) (Zampolli *et al.*, 2013; Lippert *et al.*, 2018), i.e.,

$$\Delta L_{\mathrm{TL}}(r_1,r) = 10\log_{10}\frac{r}{r_1}\ \mathrm{dB} + \alpha(r - r_1), \tag{3}$$

where α is the horizontal decay rate, related to the plane wave reflection coefficient (R) (Ainslie, 2010, p. 198) and cycle distance (r_c, the horizontal distance between successive bottom reflections) (Lippert *et al.*, 2018) according to

$$\alpha = -\frac{10\,\log_{10}|R|^2\ \mathrm{dB}}{r_c}. \tag{4}$$

If $L_E(r_1)$ and $\Delta L_{\mathrm{TL}}(r;r_1)$ are both known, Eq. (1) can be used to estimate $L_E(r)$. Specifically, for the DCS model

$$L_E(r) = L_E(r_1) - 10\,\log_{10}\frac{r}{r_1}\ \mathrm{dB} - \alpha(r - r_1). \tag{5}$$

The DCS model [Eq. (5)] is used in Fig. 1 to plot $L_{E,\mathrm{ss}}$ versus range for a pile strike sequence at the BR1 wind farm (ITAP, 2015a), for $r_1 = 234$ m, where the $L_{E,\mathrm{ss}}(r_1) = 178$ dB. The DCS prediction neatly explains the $10\log_{10}r$ (i.e., $F_{\mathrm{TL}} = r_1/r$) behavior at short range and the exponential damping beyond 1 km. This match between prediction and measurement supports the DCS theory, thus providing confidence in its predictions. By contrast, there exists no power law [i.e., no value of β in Eq. (2)] that provides a similarly close match. In addition to BR1, the suitability of DCS has been demonstrated by Lippert *et al.* (2018) for two other German sites: BARD Offshore 1 (BO1) and Global Tech 1 (GT1). The water depths for the measurement sites are listed in Table I.

The validity region of Eq. (5) is limited ultimately by the attenuation coefficient α, which is determined by the seabed reflection coefficient (Lippert *et al.*, 2018). The exponential decay ensures that when the product αr becomes excessively large, the amplitude of the Mach cone becomes negligible compared with that of near-horizontal paths, which are initially much weaker. The determination of a precise limit, which would depend on water depth and bottom type, is beyond the scope of this work. However,

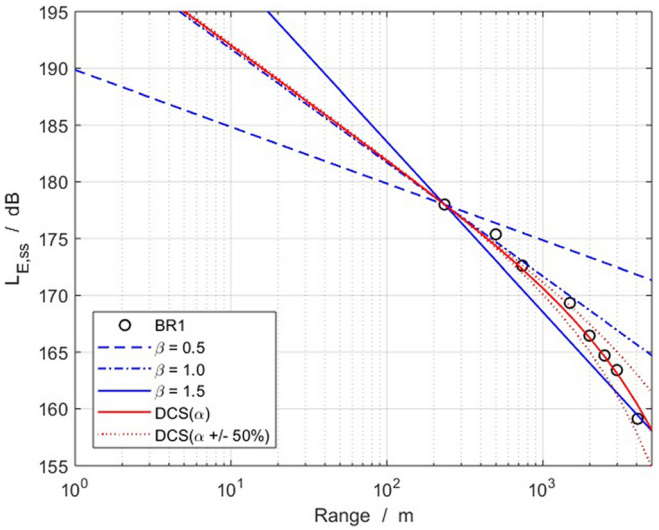

FIG. 1. (Color online) $L_{E,ss}$ (re 1 μPa^2 s) versus range using the DCS model (curved solid line). Comparison with measurements from Borkum Riffgrund 1 (Lippert *et al.*, 2018), using $r_1 = 234$ m as the intercept point. The straight dashed, dashed-dotted, and solid lines were calculated using Eq. (2) with $\beta = 0.5$, 1.0, and 1.5, respectively. Circles represent measurements. Dotted lines illustrate the uncertainty in the DCS curve resulting from a spread of $\pm 50\%$ in the attenuation coefficient (α).

Heaney *et al.* (2020) suggested a limit of $\alpha r < 20$ dB, based on predictions to 50 km from the COMPILE workshop (Lippert *et al.*, 2016). Further, the Heaney *et al.* (2020) report suggests an upper limit on the measurement distance of $\alpha r_1 < 3$ dB to limit uncertainty in the extrapolation caused by uncertainty in the value of α. For example, use of $\alpha = 1.38$ dB/km estimated for BR1 (Lippert *et al.*, 2018) results in an upper limit on r_1 of 2.2 km for the BR1 conditions. When a depth-average measurement is used, then there is no lower limit because the cylindrical spreading behavior continues up to the pile wall (Zampolli *et al.*, 2013). However, when a single depth measurement is used, the lower limit on r_1 is about three water depths (Dahl *et al.*, 2012).

III. REGRESSION ANALYSIS FOR $L_{p,pk}$, $L_{p,rms}$ AND $L_{p,eff}$

The DCS model provides a reliable means of predicting $L_{E,ss}$ (and thereby $L_{E,cum}$) up to a few kilometers (around $\alpha r \sim 20$ dB) from an impact-driven pile (Lippert *et al.*, 2018). Also of interest are $L_{p,pk}$ and $L_{p,rms}$ (e.g., for acoustic impact criteria), which cannot be calculated directly using DCS because the output of DCS is sound exposure, not sound pressure as either peak or rms. Nevertheless, a strong correlation is known to exist between $L_{E,ss}$ and $L_{p,pk}$ (Lippert *et al.*, 2015; Martin and Barclay, 2019). This correlation, and a similar one for $L_{p,rms}$, can be exploited to estimate $L_{p,pk}$ and $L_{p,rms}$ when $L_{E,ss}$ is known.

TABLE I. Water depth and pile diameter for measurement sites. U8 and Z2 are two piles at the Gemini construction site. Similarly, EL39 and EL42 are two piles at Luchterduinen.

Site	Water depth/m	Nominal pile diameter/m	Measurement report
BARD Offshore 1 (BO1)	40	3.35	OMK 1 (ITAP, 2014)
Borkum Riffgrund 1 (BR1)	27	6	OMK 3 (ITAP, 2015a)
Gemini U8	34.1	7.0	Gemini (ITAP, 2015d)
Gemini Z2	30.0	6.6	Gemini (ITAP, 2015d)
Global Tech 1 (GT1)	39.5	2.5	OMK 2 (ITAP, 2015b)
Luchterduinen EL39	21.5	5.0	Luchterduinen (ITAP, 2015c)
Luchterduinen EL42	20.6	5.0	Luchterduinen (ITAP, 2015c)

A. Measurement sites and processing

This section presents regressions for $L_{p,pk}$ and $L_{p,rms}$ using measurements from BR1, BO1, GT1 (Lippert *et al.*, 2015), and a Dutch site called Luchterduinen (ITAP, 2015c). Unless otherwise specified, mention of the name "Luchterduinen" implies use of combined data from two monopiles EL39 and EL42. Similarly, "Gemini" implies use of combined data from U8 and Z2. Medium sand was the sediment type for all the sites; BR1, BO1, and GT1 (Lippert *et al.*, 2015), Luchterduinen (ITAP, 2015c), and Gemini (ITAP, 2015d), shown in Fig. 2. Measurements from the three German sites and Luchterduinen (all except Gemini) were combined to produce a single regression equation for $L_{p,pk}$ that was valid for these four sites. The reason for excluding Gemini data from this regression analysis was to provide an independent data set for validation; thus the resulting combined regression formula was tested on Gemini (ITAP, 2015d) (Table I). For the acoustic field measurements, no noise abatement measures (e.g., bubble curtains) were applied during the piling operation. Each step is discussed below.

Acoustic data were recorded at sampling frequencies of 44.1 and 48.0 kHz and processed in the acoustic frequency band approximately between 14 Hz and 18 kHz. Hydrophones were placed at two depths, at 2 and 10 m from

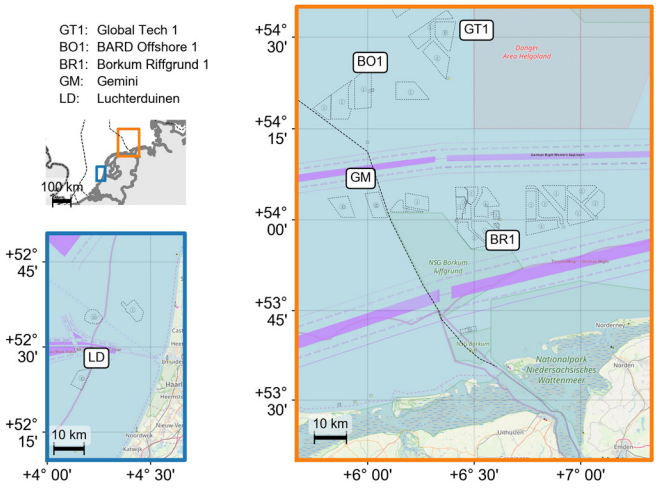

FIG. 2. (Color online) Location of the relevant wind farms. Left: Wind farm off the western Dutch coast. Right: Wind farms off the northern Dutch-German coasts (background maps from thematicmapping.org, openstreetmap.org and map.openseamap.org; shipping lanes and traffic separation scheme indicated by darker shading).

https://doi.org/10.1121/10.0001443

TABLE II. Coefficients a and b in Eq. (6). For BO1, BR1, and GT1, these are obtained from Lippert *et al.* (2015), where a is rounded to two decimal places. See surrounding text for explanation.

Site	a	b/ dB	Measurement range / km
BO1	1.40	–49.1	0.26–1.52
BR1	1.43	–49.7	0.23–4.06
GT1	1.45	–52.0	1.09–5.19
3-site average [Eq. (16)]	1.427	–50.3	0.23–5.19
Luchterduinen [Eq. (12)]	1.162	–7.3	0.75–13.75
4-site average [Eq. (15)]	1.201	–12.8	0.23–13.75

the seafloor. Data from overloaded hydrophones were identified and discarded. For further data processing details, see the measurement reports by ITAP (2014, 2015a-d).

B. Regression for German sites ($L_{p,\mathrm{pk}}$)

Lippert *et al.* (2015) demonstrated an empirical correlation between sound exposure and the peak-to-peak sound pressure ($p_{\mathrm{pk\text{-}pk}}$). However, interest lies in the zero-to-peak sound pressure (p_{pk}) or (equivalently expressed in decibels) the zero-to-peak sound pressure level ($L_{p,\mathrm{pk}}$) because this quantity is widely used to predict impact ranges and ultimately estimate the risk of underwater sound on marine life (Southall *et al.*, 2007; Southall *et al.*, 2019; Popper *et al.*, 2014; NMFS, 2018). Specifically, regression equations were obtained in the form

$$L_{p,\mathrm{pk}} = aL_{E,\mathrm{ss}} + b, \tag{6}$$

where, for each site, a and b are constants that resulted from the regression analysis, the numerical values of which are listed in Table II. The values for BO1 and BR1 are from Lippert *et al.* (2018), with the intercept adjusted to account for the ratio of p_{pk} to $p_{\mathrm{pk\text{-}pk}}$. The values for GT1 were calculated in the same way, correcting an error in the intercept a and slope b from Table I of Lippert *et al.* (2018) for this case. In Lippert *et al.* (2018), the code for GT1 incorrectly combined the zero-to-peak and peak-to-peak sound pressure values, thereby leading to slightly different coefficients for the trend line.

C. Regression for Luchterduinen site ($L_{p,\mathrm{pk}}$ and $L_{p,\mathrm{rms}}$)

1. Piling sequence

L_E measurements were available for the full piling sequences for the two monopiles EL39 and EL42 at Luchterduinen (ITAP, 2015c). The data covered the approximate range in $L_{E,\mathrm{ss}}$ of 138–178 dB (Fig. 3), thereby extending the previous range of $L_{E,\mathrm{ss}}$ values (155–170 dB), for which similar regressions were carried out by Lippert *et al.* (2015). Using an integration time of 125 ms, Martin and Barclay (2019) demonstrated a curved fit for a tilted pile in the $L_{E,\mathrm{ss}}$ range of 120–170 dB. The short integration time would explain part of the gradient change reported for weaker (more distant) signals if these were more spread out in time.

2. Correlations between $L_{p,\mathrm{pk}}$ and $L_{E,\mathrm{ss}}$

Figure 4 is a scatter plot of $L_{p,\mathrm{pk}}$ versus $L_{E,\mathrm{ss}}$ for individual hammer strikes at Luchterduinen, which shows these two metrics are linearly correlated over a 40 dB range of $L_{E,\mathrm{ss}}$ (138–178 dB).

3. Correlations between $L_{p,\mathrm{rms}}$ and $L_{E,\mathrm{ss}}$

Different definitions of signal duration can be used to determine the time-averaged sound pressure level $L_{p,\mathrm{rms}}$ of a signal with a known sound exposure level $L_{E,\mathrm{ss}}$, and the value of $L_{p,\mathrm{rms}}$ can be significantly different depending on the choice of this duration. For this study, two variants of $L_{p,\mathrm{rms}}$ were considered, one based on the 90% energy signal duration, τ_{90} (ISO, 2017) and the other on the effective signal duration, τ_{eff} (ISO, 2017). The first is

$$L_{p,90\%} = 10\log_{10}\left(\frac{P_{90}}{1\ \mu\mathrm{Pa}^2}\right)\mathrm{dB}, \tag{7}$$

and P_{90} is the mean-square sound pressure averaged over the 90% energy signal duration,

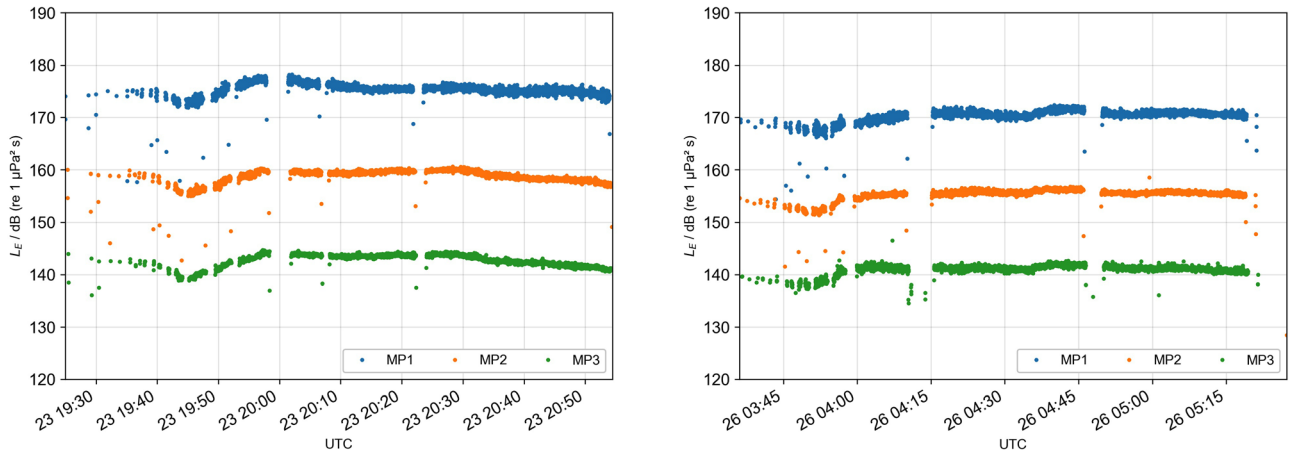

FIG. 3. (Color online) $L_{E,\mathrm{ss}}$ (re 1 μPa^2 s) versus UTC time (d h:min) at the Luchterduinen wind farm for monopiles EL39 (top) and EL42 (bottom). $L_{E,\mathrm{ss}}$ values are for three measurement ranges (at 0.8, 5.0, and 13.5 km), 2 m above the seafloor (ITAP, 2015c).

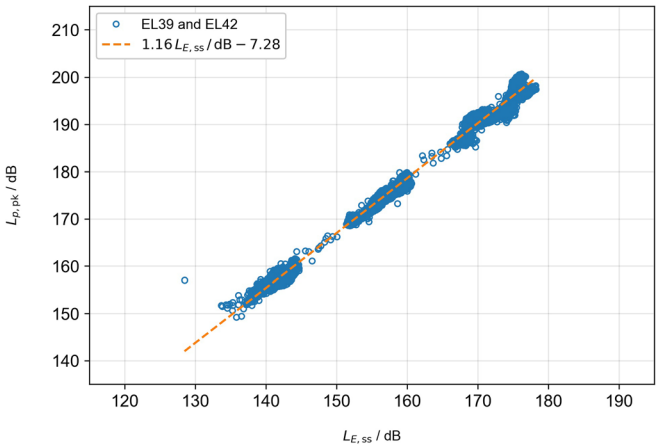

FIG. 4. (Color online) Luchterduinen: Scatter plot showing correlation between $L_{p,\mathrm{pk}}$ (re 1 μPa^2) and $L_{E,\mathrm{ss}}$ (re 1 μPa^2 s). The correlation remains linear over a 45 dB range in $L_{E,\mathrm{ss}}$. Dots are measurements; straight line is the regression (coefficient of determination $R^2 = 0.996$; residual rms = 0.95 dB).

$$P_{90} = \frac{E_{\mathrm{ss}}}{\tau_{90}/0.9}, \tag{8}$$

where E_{ss} is the sound exposure corresponding to a single hammer strike.

The second variant is

$$L_{p,\mathrm{eff}} = 10\log_{10}\left(\frac{P_{\mathrm{eff}}}{1\,\mu\mathrm{Pa}^2}\right)\mathrm{dB}, \tag{9}$$

where P_{eff} is the mean-square sound pressure of a pulse whose E_{ss} is entirely compressed into time τ_{eff} (called the effective signal duration), i.e.,

$$P_{\mathrm{eff}} = \frac{E_{\mathrm{ss}}}{\tau_{\mathrm{eff}}}. \tag{10}$$

The concept of τ_{eff} is used in sonar signal processing as a signal-weighted measure of the signal duration. The larger the value of τ_{eff}, the greater the frequency-domain resolving capability of the waveform (Burdic, 1991, Sec. 8.4.2). The value of τ_{eff} is closely related to the sound pressure kurtosis β on the interval (t_1, t_2), as (Müller *et al.*, 2020)

$$\tau_{\mathrm{eff}} \approx \frac{3}{2}\frac{t_2 - t_1}{\beta}. \tag{11}$$

The kurtosis, which can be interpreted as a measure for the variation in amplitude (Moors, 1986), is used as a measure to reflect the impulsiveness of sound. Specifically, kurtosis is used to quantify risk associated with impulsiveness of noise in humans (Goley *et al.*, 2011; Liu *et al.*, 2015, Fuente *et al.*, 2018) and chinchillas (Hamernik and Qiu, 2001).

In Fig. 5, the spread in $L_{p,90\%}$ (left-hand graph) for a fixed $L_{E,\mathrm{ss}}$ is noticeably larger than the corresponding spread in $L_{p,\mathrm{pk}}$ (Fig. 4). This spread is attributed to a spread in the 90% energy signal duration, τ_{90}. A signal consisting of two bursts (a dual pulse), caused (say) by multipath or the bounce of a hammer, will show variation in $L_{p,90\%}$ (as indicated by the spread in Fig. 5), depending continuously on the interval between the two sub-pulses, and *discontinuously* on the proportion of the total energy contained in the weaker sub-pulse. A simplified dual pulse is illustrated by Fig. 6, which represents a single hammer strike with two distinct arrivals. Therefore, $L_{p,\mathrm{eff}}$ is proposed and was investigated as an alternative to $L_{p,90\%}$ for the $L_{p,\mathrm{rms}}$. Specifically, the effective signal duration, τ_{eff}, is proposed to replace $\tau_{90}/0.9$ in Eq. (8) such that $L_{p,\mathrm{eff}}$ is calculated instead of $L_{p,90\%}$, thus precluding the need for an arbitrary choice for the duration. The effective signal duration, τ_{eff} (ISO, 2017), is strongly correlated with τ_{90}, but shows less variability, as illustrated by Fig. 5. The only source of vertical scatter in these graphs is the variation in the denominators of Eqs. (8) and (10) for fixed $L_{E,\mathrm{ss}}$. Thus, the larger scatter in $L_{p,90\%}$ is a consequence of a larger spread in τ_{90} that is not present in τ_{eff}, and use of τ_{eff} in place of $\tau_{90}/0.9$ yields a more stable metric for $L_{p,\mathrm{rms}}$.

Results for the Luchterduinen regression analysis for $L_{p,\mathrm{pk}}$, $L_{p,90\%}$, and $L_{p,\mathrm{eff}}$ are (Figs. 4 and 5)

$$L_{p,\mathrm{pk}} = 1.162L_{E,\mathrm{ss}} - 7.3\,\mathrm{dB}, \tag{12}$$

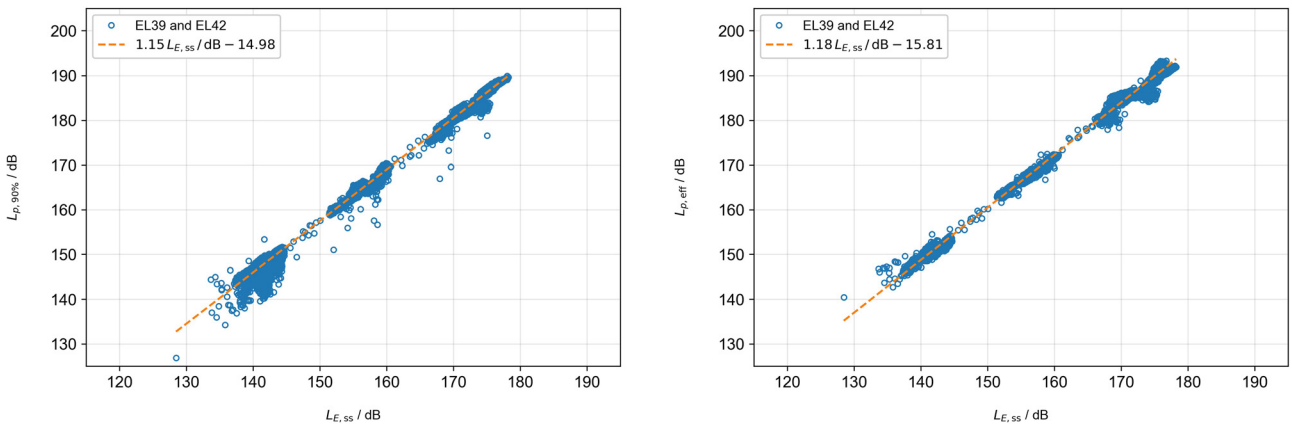

FIG. 5. (Color online) Luchterduinen: Scatter plot showing correlations between $L_{p,90\%}$ (re 1 μPa^2) and $L_{E,\mathrm{ss}}$ (re 1 μPa^2 s) (left, coefficient of determination $R^2 = 0.995$; residual rms = 1.02 dB); and between $L_{p,\mathrm{eff}}$(re 1 μPa^2) and $L_{E,\mathrm{ss}}$ (re 1 μPa^2 s) (right, coefficient of determination $R^2 = 0.997$; rms residual = 0.795 dB). Dots are measurements; straight lines are regressions.

https://doi.org/10.1121/10.0001443

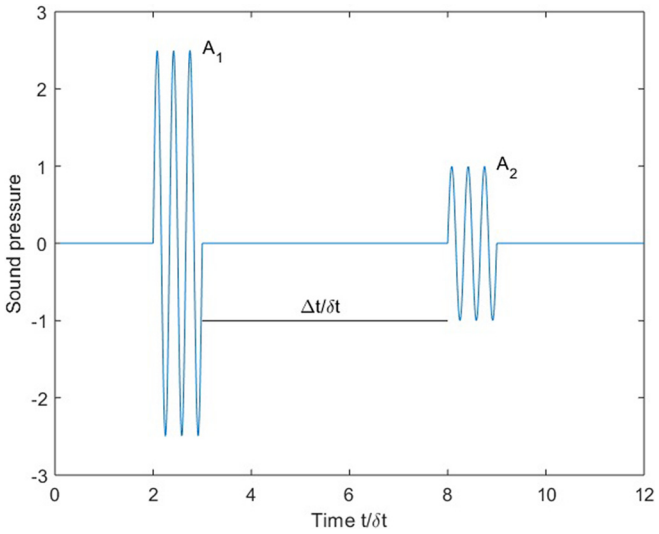

FIG. 6. (Color online) A dual-pulse waveform representing a single hammer strike with two distinct arrivals. Each sub-pulse has a duration (δt), with its respective amplitude (A_1 and A_2), and separated by a period of silence of duration (Δt). In this dual-pulse waveform, the amplitude ratio $(A_2/A_1) = 2.5$, and the sub-pulse separation $(\Delta t) = 5\delta t$.

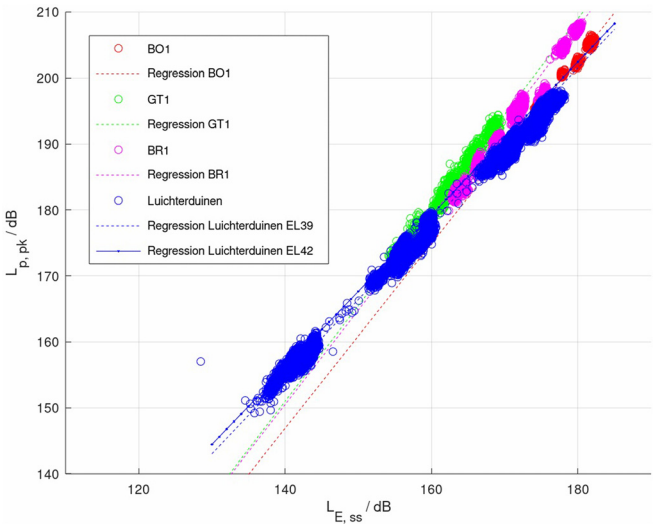

FIG. 7. (Color online) Scatter plot showing correlation between $L_{p,\mathrm{pk}}$ (re 1 μPa^2) and $L_{E,\mathrm{ss}}$ (re 1 μPa^2 s). Symbols are measurements for BO1, GT1, BR1, and Luchterduinen. The peak-to-peak quantities reported by Lippert *et al.* (2015) have been converted to their zero-to-peak equivalents according to Sec. III B.

$$L_{p,90\%} = 1.150 L_{E,\mathrm{ss}} - 15.0\,\mathrm{dB}, \tag{13}$$

and

$$L_{p,\mathrm{eff}} = 1.176 L_{E,\mathrm{ss}} - 15.8\,\mathrm{dB}, \tag{14}$$

with 95% confidence intervals in $L_{p,\mathrm{pk}}$, $L_{p,90\%}$, and $L_{p,\mathrm{eff}}$ of 1.8, 1.7, and 1.5 dB, respectively (Lippert *et al.*, 2015). Based on Fig. 5, these regressions are considered applicable in the approximate range 135–180 dB of $L_{E,\mathrm{ss}}$.

D. Regression for four sites

One final regression was carried out, the combination of $L_{p,\mathrm{pk}}$ data from Luchterduinen and the BR1, BO1, and GT1 sites, shown in Fig. 7, giving

$$L_{p,\mathrm{pk}} = 1.201 L_{E,\mathrm{ss}} - 12.8\,\mathrm{dB}. \tag{15}$$

Included in Fig. 7 are the regressions for the four sites separately.

Measurements from Gemini (ITAP, 2015d), the site not used in any of the regression analyses, were compared with the four-site regression of Eq. (15), shown in Fig. 8. Included in the figure are regressions for Luchterduinen [Eq. (12)] and the following average of the three German sites:

$$L_{p,\mathrm{pk}} = 1.427 L_{E,\mathrm{ss}} - 50.3\,\mathrm{dB}, \tag{16}$$

with a 95% confidence interval of 6.2 dB over the range 128–183 dB in $L_{E,\mathrm{ss}}$.

IV. PROPERTIES OF $L_{p,90\%}$ AND $L_{p,\mathrm{eff}}$

As mentioned in Sec. III, it is common to use τ_{90} as the averaging time for evaluating $L_{p,\mathrm{rms}}$, leading to the metric $L_{p,90\%}$. It was shown in Sec. III that $L_{p,90\%}$ is not as well correlated than $L_{p,\mathrm{pk}}$ with $L_{E,\mathrm{ss}}$. In the following, the properties of $L_{p,\mathrm{pk}}$ and $L_{p,90\%}$ are investigated. Specifically, it is shown that $L_{p,90\%}$ is unstable when the signal comprises two pulses (e.g., hammer bounce) separated in time.

The arguments P_{90} and P_{eff} of the logarithms in Eqs. (7) and (9) were evaluated for a compound signal comprising two short pulses with identical durations (δt) and different amplitudes (A_1 and A_2), separated in time by Δt (Fig. 6). The example dual-pulse test signal is not intended to capture the complexities of measured signals, but to provide insights into the causes of the observed instability in P_{90}.

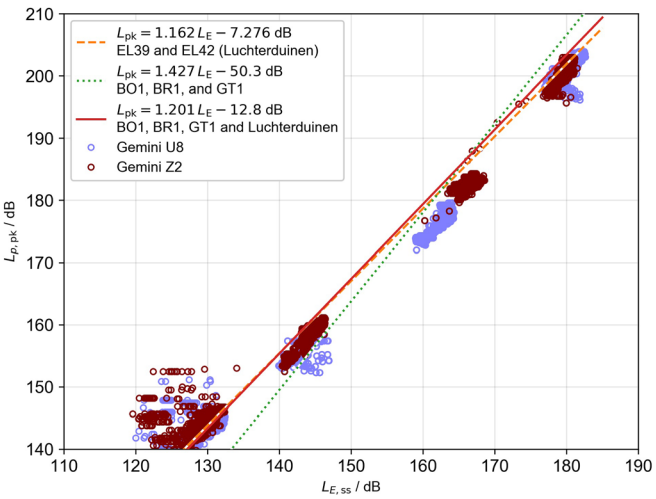

FIG. 8. (Color online) Scatter plot for the Gemini site showing correlation between $L_{p,\mathrm{pk}}$ (re 1 μPa^2) and $L_{E,\mathrm{ss}}$ (re 1 μPa^2 s). Dots are measurements for monopiles U8 and Z2 (ITAP, 2015d). The dashed line is the regression for Luchterduinen [Eq. (12)]. The dotted line is the average of the three regression formulas for the German sites [Eq. (16)]. The solid line is the combined regression for the German sites and Luchterduinen [Eq. (15)].

The sound pressure level of a transient is sometimes evaluated using an averaging time equal to the duration of the transient. However, the transient duration often is not well defined because the signal does not have a clear start and end (similar to the test signal if A_1 is either much greater than or much less than A_2). Therefore, the averaging window also is not well defined, which can create great variability in the metric values depending on small variations in definition and application of the averaging window.

The mean-square sound pressure of the signal depends on the chosen averaging window applied to the signal. In the following, P_{90} and P_{eff} were applied to the signal shape from Fig. 6 and compared with $P_{\max}$, the largest value of mean-square sound pressure during the signal, where the averaging window is one period of the sub-pulse's sine wave (Fig. 6).

A. $P_{\max}$

Ignoring edge effects, the mean-square sound pressure is ${A_1}^2/2$ during the first sub-pulse, ${A_2}^2/2$ during the second sub-pulse, and zero at all other times. An expression for $P_{\max}$ that is valid for all values of the amplitudes A_1 and A_2 is therefore

$$P_{\max} = \frac{1}{2}\max\left({A_1}^2, {A_2}^2\right). \tag{17}$$

The left-hand graph of Fig. 9 shows this quantity plotted versus A_2/A_1, normalized by dividing by ${A_1}^2/2$.

B. P_{90}

P_{90} is a measure of mean-square sound pressure that accounts for 90% of a signal's energy. The choice of averaging time is arbitrary—it could just as well have been 50% (P_{50}), 95% (P_{95}), or some other proportion of the total pulse energy. Ainslie (2010, Fig. 10.4) illustrates how the mean-square sound pressure depends on the pulse type and the choice of this percentage. The expression for P_{90} takes on a different functional form depending on whether the initial pulse contains less than 5% of the signal energy ($A_2/A_1 > \sqrt{19}$), more than 95% ($A_2/A_1 < 1/\sqrt{19}$), or some intermediate proportion ($1/\sqrt{19} < A_2/A_1 < \sqrt{19}$),

$$P_{90} = \frac{1}{2}\begin{cases} {A_1}^2 & \text{for } \dfrac{A_2}{A_1} < \dfrac{1}{\sqrt{19}} \\ \left(\dfrac{2+\Delta t/\delta t}{0.9\left({A_1}^2+{A_2}^2\right)} - \dfrac{{A_1}^2+{A_2}^2}{18\,{A_1}^2{A_2}^2}\right)^{-1} & \text{for } \dfrac{1}{\sqrt{19}} < \dfrac{A_2}{A_1} < \sqrt{19} \\ {A_2}^2 & \text{for } \dfrac{A_2}{A_1} > \sqrt{19}. \end{cases} \tag{18}$$

A large change in an acoustic metric value resulting from a negligible change in the sound field is an undesirable feature of any metric used as a correlate for the effects of underwater sound. The right side of Eq. (18) is discontinuous when

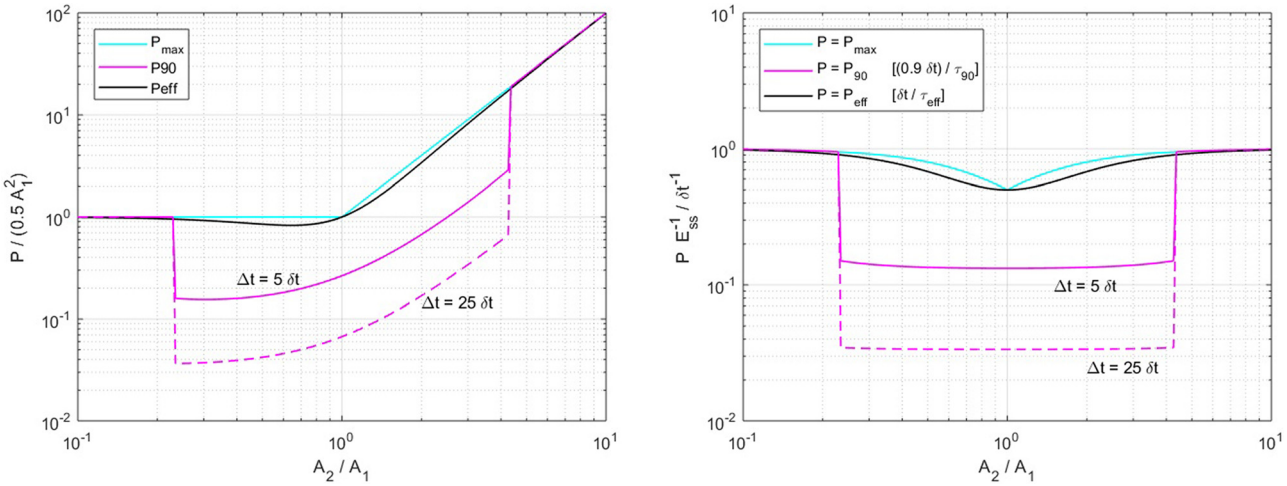

FIG. 9. (Color online) Left: Mean-square sound pressure (P) normalized the mean-square sound pressure of the first sub-pulse. $P_{\max}$ [Eq. (17)]; P_{90} [Eq. (18)]; P_{eff} [Eq. (21)]. Right: Reciprocal pulse duration $P\,E_{\text{ss}}^{-1}$, normalized by the reciprocal of the sub-pulse duration. Both are plotted versus relative sub-pulse amplitude A_2/A_1.

https://doi.org/10.1121/10.0001443

the value of A_2/A_1 passes through $1/\sqrt{19} \approx 0.229$ and $\sqrt{19} \approx 4.36$. The larger the gap between the sub-pulses relative to their duration, the larger the size of the resulting step change in P_{90} (Fig. 9). For the example dual-pulse test signal whose P was plotted in Fig. 9 for three metrics, the discontinuity in P_{90} increases from a factor of 6 (8 dB change in sound pressure level) with $\Delta t = 5\,\delta t$ to a factor of 27 (14 dB) when $\Delta t = 25\,\delta t$. When a signal consists of a larger main pulse, and a far-apart smaller sub-pulse containing about 5% of the total exposure ($0.05\,E$), τ_{90} can be unstable. When the sub-pulse exposure is less than $0.05\,E$, τ_{90} is determined by the main pulse only, while a sub-pulse slightly above $0.05\,E$ can make τ_{90} arbitrarily large and, consequently, P_{90} arbitrarily small. In Fig. 5 (upper graph) the furthest outliers are below the trend line, meaning that P_{90} is low for these pulses, which is consistent with a small number of outliers with sub-pulse energy slightly over $0.05\,E$ (Heaney *et al.*, 2020).

C. P_{eff}

The effective mean-square sound pressure, P_{eff}, is a self-weighted average of the squared sound pressure (p^2), such that the weighting function is also equal to p^2 (Müller *et al.*, 2020), and is proposed as a robust alternative to P_{90}. For the dual-pulse test signal, P_{eff} is found by substituting

$$E_{\text{ss}} = \frac{1}{2}\left(A_1^2 + A_2^2\right)\delta t \tag{19}$$

and

$$\tau_{\text{eff}} = \frac{\left(A_1^2 + A_2^2\right)^2}{A_1^4 + A_2^4}\,\delta t \tag{20}$$

into Eq. (10), giving

$$P_{\text{eff}} = \frac{1}{2}\,\frac{A_1^4 + A_2^4}{A_1^2 + A_2^2}, \tag{21}$$

which exhibits a dependence on A_2/A_1 similar to that of $P_{\max}$. The metrics P_{eff} and $P_{\max}$ are both robust, while P_{eff} has the additional benefits of avoiding the arbitrary averaging times (e.g., P_{50}, P_{90}, or P_{95},) and the discontinuous gradient at $A_2/A_1 = 1$.

$P_{\max}$, P_{90}, and P_{eff} are separately plotted as a function of the sub-pulse amplitude ratio A_2/A_1 in Fig. 9 (left). $P_{\max}$ and P_{eff} are independent of the duration ratio $\Delta t/\delta t$, while the value of P_{90} varies with $\Delta t/\delta t$, and is plotted for two Δt values, 5 and 25 δt. Also plotted in Fig. 9 (right) is the reciprocal pulse duration $P\,E_{\text{ss}}^{-1}$ with P equal to $P_{\max}$, P_{90}, or P_{eff} in the denominator. It follows from the definitions of P_{90} and P_{eff} that $E_{\text{ss}}/P_{\text{eff}}$ is equal to τ_{eff}, and E_{ss}/P_{90} is equal to $\tau_{90}/0.9$.

Figure 9 demonstrates that unless the amplitude ratio is at least 4.4 (13 dB), τ_{90} is determined by the period of silence, while P_{90} underestimates the mean-square sound pressure inside the individual pulses. The value of P_{90} changes discontinuously because τ_{90} does.

P_{90} will also be a less stable measure than P_{eff} when two strikes could accidentally be interpreted as one, for instance, when the strike interval is not known. In this case, E_{ss} will be roughly twice the intended value, while τ_{90} will be overestimated much more, leading to a low estimation of P_{90}. τ_{eff}, on the other hand, would be roughly overestimated by a factor of two, so that P_{eff} would be close to the intended value. When there is little variation between the strikes, P_{eff} is hardly influenced by the number of strikes present in a signal, so that the concept of 'a single strike' does not need to be defined to analyze P_{eff}. Figure 5 (right-hand graph) illustrates the elimination of low outliers exhibited by P_{90} in the left-hand graph. Because P_{eff} does not require the identification of individual strikes, this metric is less open to human interpretation of the signal and more applicable in situations where the individual pulses are harder to isolate; for example, corresponding to the simultaneous arrival from two nearby sources of transient sounds.

V. VALIDATION OF DCS (BR1)

Figure 10 shows measurements from BR1 of the median $L_{E,\text{ss}}$ and $L_{p,\text{pk}}$ values (ITAP, 2015a); DCS predictions for the metrics also are plotted. The reported values of $L_{p,\text{pk}}$ were the maximum from the entire series, which were then adjusted to obtain a value closer to the median $L_{p,\text{pk}}$ by subtracting the difference between the 5% and 50% $L_{E,\text{ss}}$ exceedance levels. L_E and $L_{p,\text{pk}}$ were power-averaged over the two available measurement depths. At 5 km, only one measurement depth (2 m from the seafloor) was available; therefore, averaging was not done at that range.

The lowest and highest solid curved lines are predictions of $L_{E,\text{ss}}$ and $L_{p,\text{pk}}$ using the DCS model [Eq. (5)], both

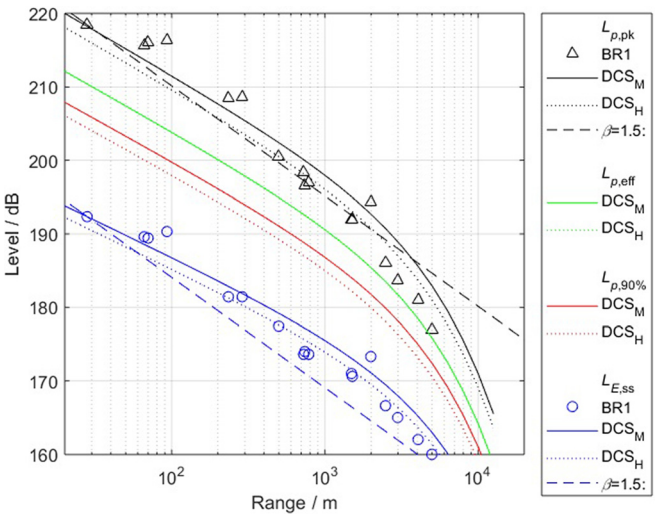

FIG. 10. (Color online) DCS for Borkum Riffgrund 1. $L_{p,\text{pk}}$ (re 1 μPa^2), $L_{p,\text{eff}}$(re 1 μPa^2), $L_{p,90\%}$(re 1 μPa^2), and $L_{E,\text{ss}}$ (re 1 μPa^2 s) versus range. Symbols are measurements ($L_{E,\text{ss}}$ BR1 and $L_{p,\text{pk}}$ BR1); curved lines are DCS predictions using Eqs. (5) ($L_{E,\text{ss}}$), (15) ($L_{p,\text{pk}}$), (13) ($L_{p,90\%}$), and (14) ($L_{p,\text{eff}}$), with sound exposure at $r_1 = 28$ m estimated by averaging over the two measurement depths [$E(r_1) = E_M(r_1)$, solid] and over the water depth [$E(r_1) = E_H(r_1)$ using Eq. (22), dotted] and $\alpha = 1.38$ dB/km (Lippert *et al.*, 2018); dashed lines are power law predictions with $\beta = 1.5$ ($L_{E,\text{ss}}$, and $L_{p,\text{pk}}$).

of which follow the trend of the measurements from 30 m to 5 km. The DCS lines are curved because of the exponential decay. The corresponding dashed lines are estimates of $L_{E,\mathrm{ss}}$ and $L_{p,\mathrm{pk}}$ using the power law [Eq. (2)] with $\beta = 1.5$, as recommended by Buehler *et al.* (2015). The DCS curves and power law $L_{E,\mathrm{ss}}$ lines were forced to match the $L_{E,\mathrm{ss}}$ measurement at 28 m. The power law $L_{p,\mathrm{pk}}$ line was forced to match the $L_{p,\mathrm{pk}}$ measurement at the same distance, but the DCS estimates of $L_{p,\mathrm{pk}}$ and $L_{p,\mathrm{rms}}$ require only the $L_{E,\mathrm{ss}}$ measurement. Relative to the measurements, the power law consistently underestimates $L_{E,\mathrm{ss}}$ between 100 m and 2 km, and overestimates $L_{p,\mathrm{pk}}$ at ranges exceeding 3 km. DCS results in accurate estimations of $L_{E,\mathrm{ss}}$ and $L_{p,\mathrm{pk}}$ at all ranges considered, with rms errors of 2.46 and 3.39 dB, respectively. By comparison, the corresponding ($\beta = 1.5$) power law rms errors are 3.90 and 3.65 dB.

Also shown in Fig. 10 are estimates of $L_{p,90\%}$ [Eq. (13)] and $L_{p,\mathrm{eff}}$ [Eq. (14)]. While a systematic validation of the empirical regressions for $L_{p,\mathrm{pk}}$ and $L_{p,\mathrm{rms}}$ is needed, their use permits extrapolation from $L_{E,\mathrm{ss}}$ to obtain estimates of $L_{p,\mathrm{pk}}$ and $L_{p,\mathrm{rms}}$.

The choice of $r_1 = 28$ m is less than the minimum distance of 3.3 water depths recommended by Dahl and Reinhall (2012). Thus, some caution is needed in estimating the depth-averaged sound exposure at this distance, E_{ss} (28 m). If the measurement depths are inside the Mach cone, there is risk of overestimating the depth-averaged sound exposure at r_1, while measurements outside the Mach cone may underestimate it. If E_{M} is the (depth-averaged) sound exposure inside the Mach cone where both receivers were placed, the average for the entire water column can be estimated by neglecting the sound outside the Mach cone,

$$E_H(r_1) = (1 - r_1 \tan\theta/H)\, E_{\mathrm{M}}(r_1), \tag{22}$$

where H is the water depth. For the scenario based on BR1, $10\log_{10}E_{\mathrm{M}}\,\mathrm{dB} = 10\log_{10}E_H\,\mathrm{dB} + 1.6\,\mathrm{dB}$. This change would have the benefit of reducing the $L_{E,\mathrm{ss}}$ and $L_{p,\mathrm{pk}}$ rms errors to 2.09 and 3.24 dB, respectively (Fig. 10, dotted lines).

VI. RANGE TO INJURY THRESHOLD FOR FISHES

A. Guidelines

Injury to fishes with and without a swim bladder from impact pile driving was investigated by Halvorsen *et al.* (2011, 2012b), Halvorsen *et al.*, 2012a), and Casper *et al.* (2012), Casper *et al.* (2013a), and Casper *et al.* (2013b), whose findings were used as the basis for guidelines by Popper *et al.* (2014). Table III lists the injury thresholds for $L_{p,\mathrm{pk}}$ and (cumulative) unweighted sound exposure level ($L_{E,\mathrm{cum}}$) for pile driving, as recommended by Popper *et al.* (2014). The guideline thresholds depend on whether a swim bladder is present and involved in hearing. The data for these guidelines used 960 hammer strikes (except for mortal injury in the fish without a swim bladder, which received 1920 strikes and had no observed injuries). The number of hammer strikes and the $L_{E,\mathrm{ss}}$ are important variables to include when reporting and investigating $L_{E,\mathrm{cum}}$. In both cases, the strike rate was 40 min^{-1}.

B. Impact ranges

1. Impact range versus number of strikes

Impact ranges were calculated for BR1 with up to 7000 hammer strikes. This is roughly the maximum number that can be expected in 24 h during an offshore piling operation (ITAP, 2015d). Estimated impact ranges, $R_{\mathrm{impact}}(N)$, for mortal and recoverable injury for fishes are compared in Figs. 11 and 12 (top, SB0; middle, SB1; bottom, SB2). The impact ranges for $L_{p,\mathrm{pk}}$, shown as vertical bars, were estimated as the intersection between each guideline threshold and the $L_{p,\mathrm{pk}}$ versus range curve. Impact range based on $L_{E,\mathrm{cum}}$ increases with increasing number of hammer strikes N. For all values of N up to 7000 strikes, the $L_{E,\mathrm{cum}}$ impact ranges were estimated as the intersection between each threshold and the $L_{E,\mathrm{cum}}$ versus range curve, and they are plotted in Figs. 11 and 12. Impact ranges were calculated twice for each threshold, for DCS [Eq. (5) with $\alpha = 1.38$ dB/km] and power law [Eq. (2) with $\beta = 1.5$] separately, using $r_1 = 28$ m for both. The power law results in the straight diagonal lines in Figs. 11 and 12, while—as with Fig. 10—the DCS lines are curved because of exponential decay.

The main results of Figs. 11 and 12 are summarized in Table IV. Results are listed with and without a hypothetical noise abatement measure, resulting in a 10 dB reduction at all ranges. For this example, when the number of hammer strikes exceeded 1000, the power law consistently underestimated the impact range compared to the DCS prediction by a factor of approximately 2.7 for fishes with a swim bladder. This can be seen for SB2 recoverable injury, when $N = 3\,000$. When applying DCS, the calculated impact range

TABLE III. Injury thresholds by Popper *et al.* (2014) for mortal and recoverable injury for fish groups based on data from 960 hammer strikes (SB1 and SB2) and 1920 strikes (SB0).

Fish hearing group	Metric	Mortality and potential mortal injury	Recoverable injury
SB0: No swim bladder	$L_{E,\mathrm{cum}}$ (re 1 $\mu\mathrm{Pa}^2$ s)	>219 dB	>216 dB
(particle motion detection)	$L_{p,\mathrm{pk}}$ (re 1 $\mu\mathrm{Pa}^2$)	>213 dB	>213 dB
SB1: Swim bladder is not	$L_{E,\mathrm{cum}}$ (re 1 $\mu\mathrm{Pa}^2$ s)	210 dB	203 dB
involved in hearing (particle motion detection)	$L_{p,\mathrm{pk}}$ (re 1 $\mu\mathrm{Pa}^2$)	>207 dB	>207 dB
SB2: Swim bladder involved in hearing	$L_{E,\mathrm{cum}}$ (re 1 $\mu\mathrm{Pa}^2$ s)	207 dB	203 dB
(primarily pressure detection)	$L_{p,\mathrm{pk}}$ (re 1 $\mu\mathrm{Pa}^2$)	>207 dB	>207 dB

https://doi.org/10.1121/10.0001443

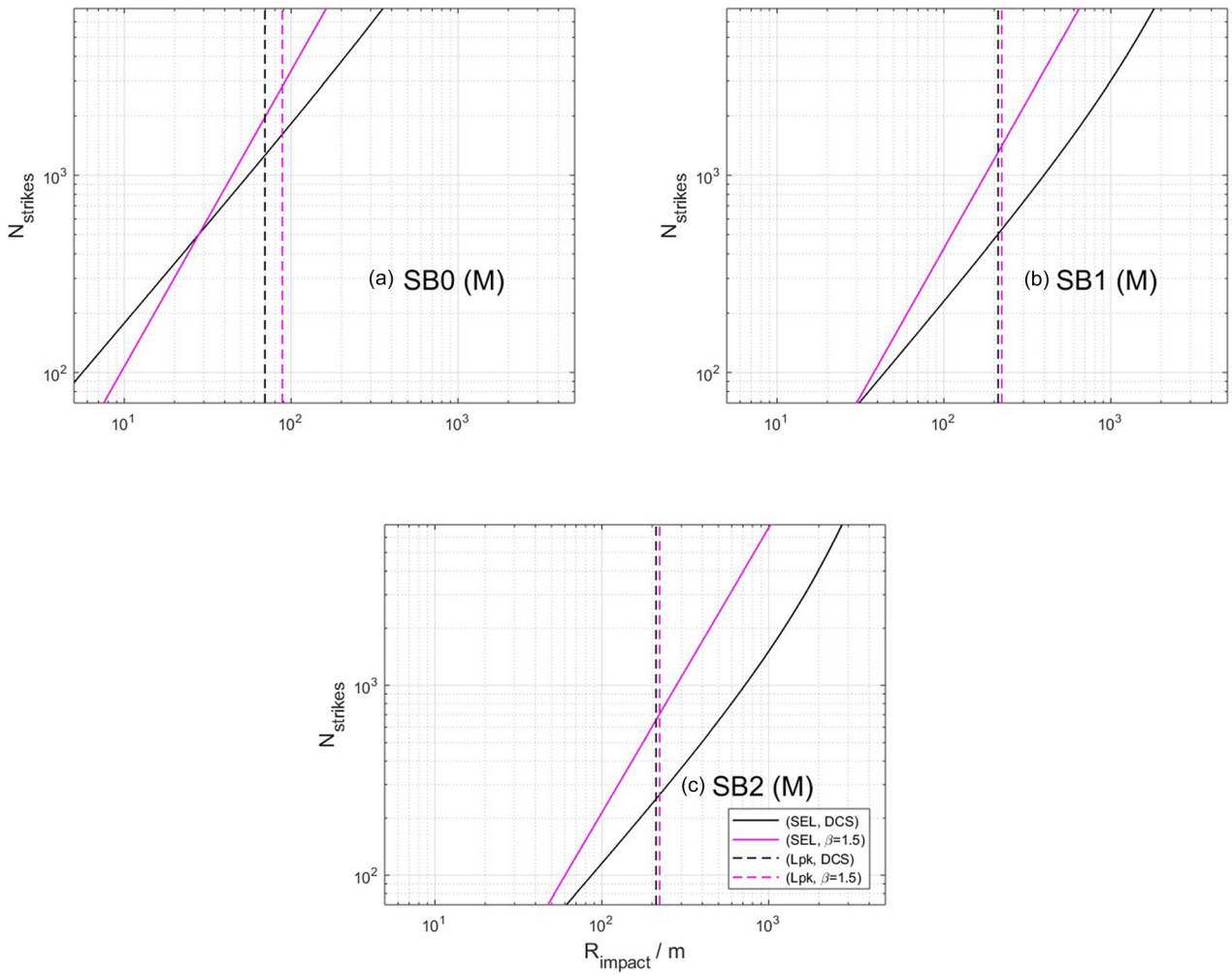

FIG. 11. (Color online) Borkum Riffgrund 1: Number of hammer strikes versus mortal injury range $R_{\text{impact}}(N)$ for three fish groups, calculated using DCS with $\alpha = 1.38$ dB/km and power law with $\beta = 1.5$. SB0, no swim bladder; SB1, swim bladder not involved; SB2, swim bladder involved. Vertical lines indicate the impact range for $L_{p,\text{pk}}$. Straight diagonal lines indicate the impact range for $L_{E,\text{cum}}$ using the power law. Curved diagonal lines indicate the impact range for $L_{E,\text{cum}}$ using DCS.

was 2870 m, while the power law predicted an impact range of less than 1080 m. In this situation, use of Eq. (2) with $\beta = 1.5$ would underestimate the affected area by a factor of $(2\,870/1\,080)^2 \approx 7$.

2. Estimated impact zone per pile

The impact zones for the fish group SB2 are considered next, using $L_{E,\text{cum}}$ thresholds for recoverable injury (203 dB) and mortal injury (207 dB). The $L_{E,\text{cum}}$ thresholds were based on 3500 hammer strikes per pile. The impact ranges from Table IV are 1.8 km for mortal injury and 3.1 km for recoverable injury, corresponding to impact areas of 10 and 30 km,^{2} respectively. With a 10 dB abatement, the impact ranges reduced to 0.29 km for mortal injury and 0.65 km for recoverable injury, corresponding to areas of 0.3 and 1.3 km,^{2} respectively. Hence the 10 dB abatement reduced the maximum impact range by 79% and area by 96%.

For the Block Island site, which used 8000 hammer strikes with a hammer energy of 0.392 MJ and pile diameter 1.52 m, Martin and Barclay (2019) estimated the impact range for $L_{E,\text{cum}}$ recoverable injury to be 0.425 km, implying $L_{E,\text{ss}}$ of 164.0 dB at that distance. This is ~15 dB lower than at the same range at BR1 (Fig. 10), thus explaining the shorter recoverable injury range at Block Island, even for the larger number of strikes (8000).

We attribute the larger $L_{E,\text{ss}}$ for BR1 conditions to a larger pile (6 m) and higher hammer energy (estimated to be in the range 0.9–1.5 MJ, based on measurements for similar piles in the North Sea (ITAP, 2015c,d,). The application of 3500 hammer strikes implies $L_{E,\text{ss}}$ of 171.6 and 167.6 dB for mortal and recoverable injury, respectively. These $L_{E,\text{ss}}$ values are 5.6 dB lower than those used by Halvorsen *et al.* (2012a) to determine the $L_{E,\text{cum}}$ thresholds based on 960 strikes used for the Popper *et al.* (2014) guidelines (Table III). They are also 3.6 dB higher than the $L_{E,\text{ss}}$ values implied by Martin and Barclay's use of 8000 strikes.

The above estimates are based on Figs. 11 and 12 and Table IV, which apply the solid curves from Fig. 10 using $E(r_1) = E_{\text{M}}(r_1)$. For the reasons described in Sec. V, this approach might overestimate $E(r_1)$ and the corresponding effect distances. Application of the dotted lines [for

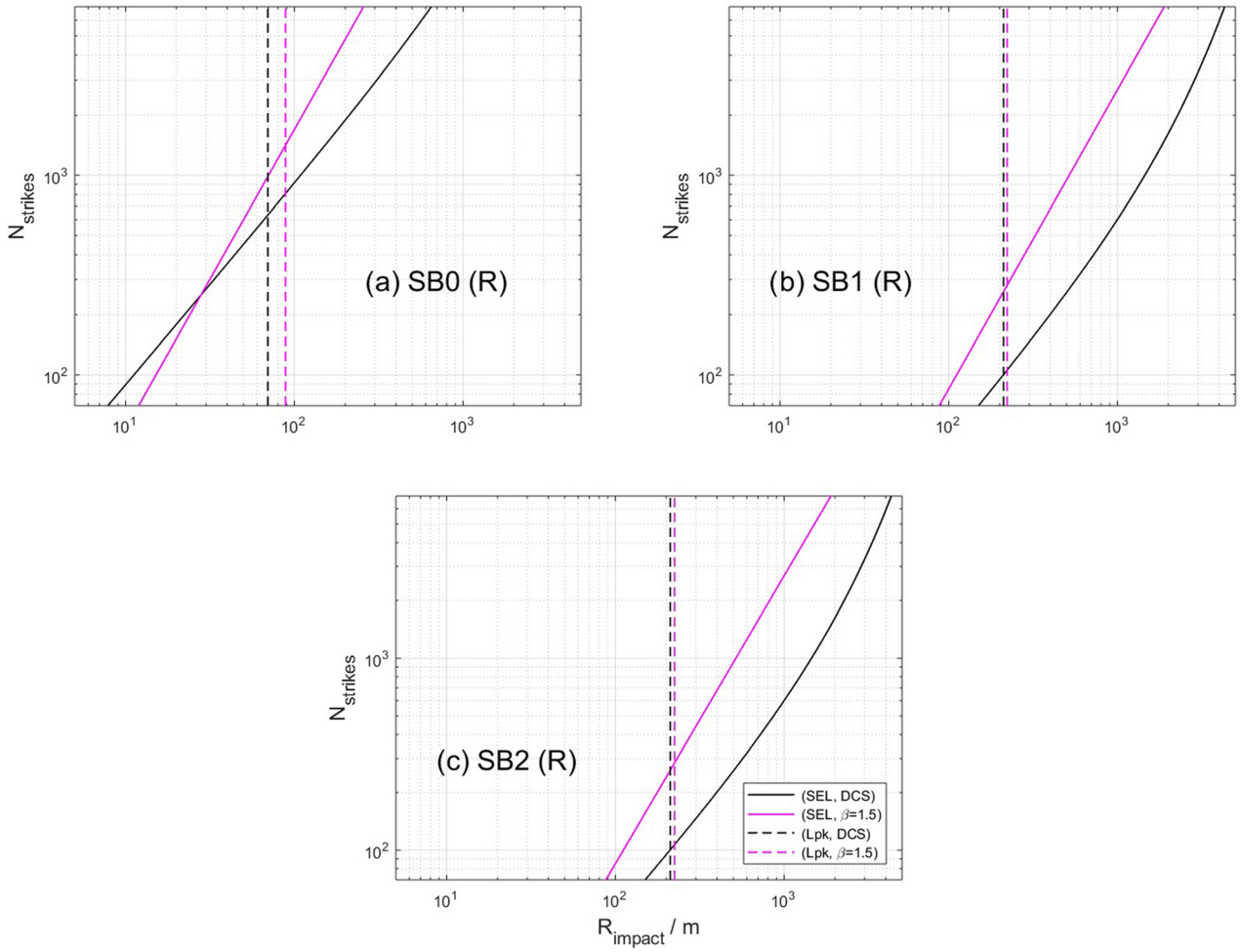

FIG. 12. (Color online) Borkum Riffgrund 1: Number of hammer strikes versus recoverable injury range $R_{\text{impact}}(N)$ for three fish groups, calculated using DCS with $\alpha = 1.38\,\text{dB/km}$ and power law with $\beta = 1.5$. SB0, no swim bladder; SB1, swim bladder not involved; SB2, swim bladder involved. Vertical lines indicate the impact range for $L_{p,\text{pk}}$. Straight diagonal lines indicate the impact range for $L_{E,\text{cum}}$ using the power law. Curved diagonal lines indicate the impact range for $L_{E,\text{cum}}$ using DCS. The middle and lower graphs are identical because the recoverable injury thresholds for SB1 and SB2 are equal (Table III).

TABLE IV. Borkum Riffgrund 1 (water depth 28 m; medium sand sediment): Estimated injury ranges (m) to $L_{E,\text{cum}}$ and $L_{p,\text{pk}}$ thresholds by application of DCS. Abatement of 0 dB corresponds to the situation portrayed by Figs. 11 and 12, i.e., with $L_{\text{E,ss}}$ (re 1 μPa^2 s) = 191.8 dB at 28 m, while 10 dB abatement corresponds to $L_{E,\text{ss}} = 181.8$ dB at 28 m.

	Estimated injury range / m											
	Fish group:	SB0				SB1				SB2			
	Injury type:	Mortal		Recoverable		Mortal		Recoverable		Mortal		Recoverable	
Number of strikes	Abatement:	0 dB	10 dB	0 dB	10 dB	0 dB	10 dB	0 dB	10 dB	0 dB	10 dB	0 dB	10 dB
						$L_{E,\text{cum}}$							
2		-	-	-	-	-	-	4	-	-	-	4	-
7		-	-	-	-	3	-	16	-	6	-	16	-
20		-	-	-	-	9	-	44	4	18	-	44	4
70		<4	-	<8	-	31	3	150	16	61	6	150	16
200		<11	-	<22	-	87	9	398	44	170	18	398	44
700		<39	<4	<77	<8	287	31	1 122	150	533	61	1 122	150
2 000		<109	<11	<211	<22	721	87	2 273	398	1 234	170	2 273	398
3 500		<186	<20	<354	<39	1 204	150	3 103	647	1 816	287	3 103	647
7 000		<355	<39	<648	<77	1 818	287	4 317	1122	2 748	533	4 317	1 122
						$L_{p,\text{pk}}$							
n/a		<70	<7	<70	<7	<211	<22	<211	<22	<211	<22	<211	<22

https://doi.org/10.1121/10.0001443

$E(r_1) = E_H(r_1)$] would result in systematically lower estimates of $L_{E,\mathrm{ss}}$ and $L_{p,\mathrm{pk}}$ by 1.6 and 1.9 dB, respectively. Applying this correction would reduce estimated effect distances by between 18% (applicable to the longest impact range of 3.1 km, which would be reduced to 2.5 km) and 36% (applies to $L_{p,\mathrm{pk}}$ in the cylindrical spreading region, such that 211 m would be reduced to 136 m). The corresponding reduction in impact area is between 33% and 59%.

3. Comparison with power law

The power law underestimates the ($L_{E,\mathrm{cum}}$) impact range because it underestimates the sound exposure E at ranges $r > r_1$. Specifically, the power law is [using $\beta = 1.5$ in Eq. (2)]

$$\frac{E_{\beta=1.5}(r)}{E(r_1)} = \left(\frac{r}{r_1}\right)^{-3/2}, \tag{23}$$

whereas the range dependence according to the more accurate DCS [Eq. (5)] is

$$\frac{E_{\mathrm{DCS}}(r)}{E(r_1)} = \left(\frac{r}{r_1}\right)^{-1} \mathrm{e}^{-\alpha(r-r_1)}. \tag{24}$$

Taking the ratio of Eq. (23) to Eq. (24) gives

$$\frac{E_{\mathrm{DCS}}}{E_{\beta=1.5}} = \left(\frac{r}{r_1}\right)^{1/2} \mathrm{e}^{\alpha(r_1-r)}, \tag{25}$$

and the power law therefore overestimates by the same ratio the number of strikes (at fixed E_{ss}) that result in reaching a specified threshold (we refer to this number as the "threshold number" of strikes). The value of the ratio depends on the value of r_1 (Fig. 13). For $r < r_1$, the situation is reversed, with the threshold number of strikes being underestimated. At r_1, the DCS and power law estimates are the same (234 m in Fig. 1) because r_1 is the fixed measurement position from which both DCS and power law are extrapolated. At $r < r_1$, $L_{E,\mathrm{cum}}$ is overestimated, so the threshold number is underestimated. At $r > r_1$, $L_{E,\mathrm{cum}}$ (initially) is underestimated, and the threshold number is overestimated.

VII. CONCLUSIONS

We draw two main conclusions, first related to the suitability of DCS for estimating L_E, $L_{p,\mathrm{pk}}$, and $L_{p,\mathrm{rms}}$, and second related to evaluating the range to injury threshold in fishes.

A. The DCS is applicable to ranges at least up to 5 km

Both power law [Eq. (2)] and DCS [Eq. (5)] provide a mechanism for extrapolating from a measurement of L_E at a specified range, denoted r_1. We have compared the accuracy of these two methods for two different values of r_1: 28 and 234 m. In both cases, the power law with $\beta = 1.5$ overestimates $L_E(r)$ for $r < r_1$ and underestimates $L_E(r)$ for $r > r_1$,

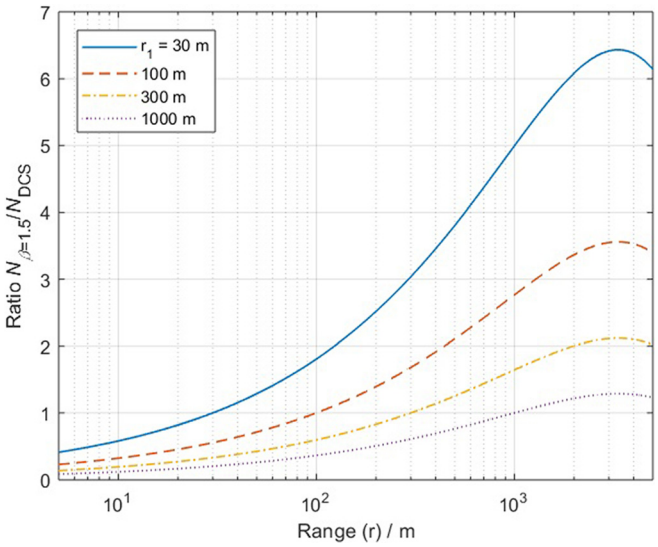

FIG. 13. (Color online) Ratio by which the number of strikes required to reach a sound exposure threshold is overestimated by the power law with $\beta = 1.5$ [using $\alpha = 1.38$ dB/km in Eq. (25)]. This ratio decreases with increasing value of r_1, as indicated by the legend. When the ratio is less than 1, the number of strikes is underestimated.

at least up to the maximum measurement range available (5 km), whereas DCS reproduces the measured values in this range.

Both $L_{p,\mathrm{pk}}$ and $L_{p,\mathrm{rms}}$ are linearly correlated with L_E over a range of $L_{E,\mathrm{ss}}$ between 138 and 178 dB. The correlation with $L_{p,\mathrm{rms}}$ shows more scatter than for $L_{p,\mathrm{pk}}$ when the 90% energy signal duration is chosen for the averaging time. This scatter is caused by a fundamental instability in the τ_{90} metric, leading to a corresponding instability in $L_{p,90\%}$. A proposed solution is to instead apply τ_{eff} for the averaging time, which was shown to be a more robust measure of signal duration and greatly reduced data scatter. As the values of $L_{p,\mathrm{eff}}$ are consistently higher than those of $L_{p,90\%}$, risk thresholds could be adjusted upwards to avoid an overly precautionary requirement.

B. The range to the recoverable injury threshold in fishes is up to 3.1 km

The range to injury threshold was considered for fishes from impact pile driving using the guidelines of Popper *et al.* (2014). The scenarios assumed the same construction conditions as at the BR1 wind farm. The following conclusions based on DCS were reached. For both mortal and recoverable injury, the predicted range to the $L_{p,\mathrm{pk}}$ threshold ($L_{p,\mathrm{pk}}$ impact range) was 211 m for fishes with a swim bladder (SB1 or SB2) and 70 m for fishes without a swim bladder (SB0), independent of the number of strikes. The predicted range to the $L_{E,\mathrm{cum}}$ threshold ($L_{E,\mathrm{cum}}$ impact range) depends on the number of strikes: For up to 100 hammer strikes, the $L_{E,\mathrm{cum}}$ impact ranges were smaller than the corresponding $L_{p,\mathrm{pk}}$ ranges for all fish groups; for more than 2000 strikes, the $L_{E,\mathrm{cum}}$ impact ranges were larger than the corresponding $L_{p,\mathrm{pk}}$ ranges for all fish groups.

For 3500 hammer strikes, the predicted range to $L_{E,\mathrm{cum}}$ threshold for recoverable and mortal injury was 3.1 and 1.8 km, respectively, corresponding to impact areas of 30 km^2 for recoverable injury and 10 km^2 for mortal injury. By comparison, the power law ($\beta = 1.5$) underestimates the impact area by a factor 7 for conditions corresponding to construction of BR1, with $r_1 = 28$ m. An investigation of the application of a noise abatement mitigation measure that reduced noise by 10 dB at all ranges was found to decrease the maximum impact range by 79% and area by 96%.

The above estimates are based on the solid curves from Fig. 10, which use $E(r_1) = E_{\mathrm{M}}(r_1)$. This approach might overestimate $E(r_1)$ and the corresponding effect distances. Application of the dotted lines [for $E(r_1) = E_H(r_1)$] would result in systematically lower estimates of $L_{E,\mathrm{ss}}$ and $L_{p,\mathrm{pk}}$ by 1.6 and 1.9 dB, respectively. Applying this correction would reduce estimated effect distances by between 18% (reducing the longest impact range of 3.1 km to 2.5 km) and 36%. The corresponding reduction in impact area is between 33% and 59%.

ACKNOWLEDGMENTS

This work was sponsored by the U.S. Bureau of Ocean Energy Management, under contract number M17PD00003.

Ainslie, M. A. (**2010**). *Principles of Sonar Performance Modeling* (Springer-Verlag, Heidelberg), pp. 198, 535.

Ainslie, M. A., Dahl, P. H., de Jong, C. A. F., and Laws, R. M. (**2014**). "Practical spreading laws: The snakes and ladders of shallow water acoustics," in *Proceedings of the 2nd International Conference and Exhibition on Underwater Acoustics*, June 22–27, Rhodes, Greece, pp. 22–27.

Ainslie, M. A., de Jong, C. A., Robinson, S. P., and Lepper P. A. (**2012**). "What is the source level of pile-driving noise in water?," in *The Effects of Noise on Aquatic Life*, edited by A. N. Popper and A. Hawkins (Springer, New York), pp. 445–448.

Buehler, D., Oestman, R., Reyff, J., Pommerenck, K., and Mitchell, B. (**2015**). "Technical guidance for assessment and mitigation of the hydroacoustic effects of pile driving on fish," California Department of Transportation (Caltrans) Report No. CTHWANP-RT-15-306.01.01 (California Department of Transportation, Sacramento, CA), pp. 4–21.

Burdic, W. S. (**1991**). *Underwater Acoustic System Analysis* (Prentice-Hall, Englewood Cliffs, NJ), p. 222.

Casper, B. M., Halvorsen, M. B., Carlson, T. J., and Popper, A. N. (**2017**). "Onset of barotrauma injuries related to number of pile driving strike exposures in hybrid striped bass," J. Acoust. Soc. Am. **141**, 4380–4387.

Casper, B. M., Halvorsen, M. B., Matthews, F., Carlson, T. J., and Popper, A. N. (**2013a**). "Recovery of barotrauma injuries resulting from exposure to pile driving sounds in two sizes of hybrid striped bass," PLoS One **8**(9), e73844.

Casper, B. M., Popper, A. N., Matthews, F., Carlson, T. J., and Halvorsen, M. B. (**2012**). "Recovery of barotrauma injuries in Chinook salmon, *Oncorhynchus tshawytscha* from exposure to pile driving sound," PLoS One **7**(6), e39593.

Casper, B. M., Smith, M. E., Halvorsen, M. B., Sun, H., Carlson, T. J., and Popper, A. (**2013b**). "Effects of exposure to pile driving sounds on fish inner ear tissues," Comp. Biochem. Physiol. A **166**, 352–360.

Dahl, P. H., Reinhall, P. G., and Farrell D. M. (**2012**). "Transmission loss and range, depth scales associated with impact pile driving," in *Proceedings of the 11th European Conference on Underwater Acoustics*, July 2–6, Edinburgh, UK (Vol. 34, pp. 1860–1867).

Dähne, M., Gilles, A., Lucke, K., Peschko, V., Adler, S., Krügel, K., Sundermeyer, J., and Siebert, U. (**2013**). "Effects of pile-driving on harbour porpoises (*Phocoena phocoena*) at the first offshore wind farm in Germany," Environ. Res. Lett. **8**(2), 025002.

Finneran, J. J. (**2015**). "Noise-induced hearing loss in marine mammals: A review of temporary threshold shift studies from 1996 to 2015," J. Acoust. Soc. Am. **138**, 1702–1726.

Finneran, J. J., Dear, R., Carder, D. A., and Ridgway, S. H. (**2003**). "Auditory and behavioral responses of California sea lions (*Zalophus californianus*) to single underwater impulses from an arc-gap transducer," J. Acoust. Soc. Am. **114**, 1667–1677.

Finneran, J. J., Schlundt, C. E., Branstetter, B. K., Trickey, J. S., Bowman, V., and Jenkins, K. (**2015**). "Effects of multiple impulses from a seismic air gun on bottlenose dolphin hearing and behavior," J. Acoust. Soc. Am. **137**, 1634–1646.

Finneran, J. J., Schlundt, C. E., Carder, D. A., Clark, J. A., Young, J. A., Gaspin, J. B., and Ridgway, S. H. (**2000**). "Auditory and behavioral responses of bottlenose dolphins (*Tursiops truncatus*) and a beluga whale (*Delphinapterus leucas*) to impulsive sounds resembling distant signatures of underwater explosions," J. Acoust. Soc. Am. **108**, 417–431.

Finneran, J. J., Schlundt, C. E., Dear, R., Carder, D. A., and Ridgway, S. H. (**2002**). "Temporary shift in masked hearing thresholds in odontocetes after exposure to single underwater impulses from a seismic watergun," J. Acoust. Soc. Am. **111**, 2929–2940.

Fuente, A., Qiu, W., Zhang, M., Xie, H., Kardous, C. A., Campo, P., and Morata, T. C. (**2018**). "Use of the kurtosis statistic in an evaluation of the effects of noise and solvent exposures on the hearing thresholds of workers: An exploratory study," J. Acoust. Soc. Am. **143**(3), 1704–1710.

Goley, G. S., Song, W. J., and Kim, J. H. (**2011**). "Kurtosis corrected sound pressure level as a noise metric for risk assessment of occupational noises," J. Acoust. Soc. Am. **129**(3), 1475–1481.

GARFO (**2016**). "Acoustic tool: Analyzing the effects of pile driving on ESA-listed species in the Greater Atlantic Region, Excel spreadsheet," U.S. Department of Commerce, National Oceanic and Atmospheric Administration, National Marine Fisheries Services, http://www.greateratlantic.fisheries.noaa.gov/protected/section7/guidance/consultation/index.html (Last viewed May 1, 2018).

Halvorsen, M. B., Casper, B. M., Matthews, F., Carlson, T. J., and Popper, A. N. (**2012a**). "Effects of exposure to pile-driving sounds on the lake sturgeon, Nile tilapia and hogchoker," Proc. R. Soc. B: Biol. Sci. **279**(1748), 4705–4714.

Halvorsen, M. B., Casper, B. M., Woodley, C. M., Carlson, T. J., and Popper, A. N. (**2011**). "Predicting and mitigating hydroacoustic impacts on fish from pile installations," NCHRP Research Results Digest 363, Project 25-28, National Cooperative Highway Research Program. Transportation Research Board (National Academy of Sciences, Washington, DC).

Halvorsen, M. B., Casper, B. M., Woodley, C. M., Carlson, T. J., and Popper, A. N. (**2012b**). "Threshold for onset of injury in Chinook salmon from exposure to impulsive pile driving sounds," PLoS One **7**(6), e38968.

Hamernik, R. P., and Qiu, W. (**2001**). "Energy-independent factors influencing noise-induced hearing loss in the chinchilla model," J. Acoust. Soc. Am. **110**(6), 3163–3168.

Heaney, K. D., Ainslie, M. A., Halvorsen, M. B., Seger, K. D., Müller, R. A. J., Nijhof, M. J. J., and Lippert, T. (**2020**). "A parametric analysis and sensitivity study of the acoustic propagation for renewable energy sources and projects report," U.S. Department of the Interior, Bureau of Ocean Energy Management, OCS Study BOEM 2020-011, prepared by CSA Ocean Sciences Inc. (CSA Ocean Sciences, Stuart, FL), p. 165.

Heitmann, K. (**2016**). "Vorhersage des Unterwasserschalls bei Offshore-Rammarbeiten unter Berücksichtigung von Schallminderungsmaßnahmen" ("Prediction of underwater noise during offshore pile driving, taking noise reduction measures into account"), Ph.D. thesis, Hamburg University of Technology, Hamburg, Germany.

ISO (**2015**). ISO 1683:2015, *Acoustics—Preferred Reference Values for Acoustical and Vibratory Levels* (International Organization for Standardization, Geneva, Switzerland).

ISO (**2017**). ISO 8405:2017, *Underwater Acoustics—Terminology* (International Organization for Standardization, Geneva, Switzerland).

ITAP (**2014**). "Offshore Messkampagne 1 (OMK 1) für das Projekt BORA im Windpark BARD Offshore 1" ["Offshore measurement campaign 1 (OMK1) for the project BORA at the offshore-wind farm Bard Offshore 1"], Version 7, Project Number: 1924 12 bm (ITAP, Wein, Austria).

ITAP (**2015a**). "Offshore Messkampagne 3 (OMK 3) für das Projekt BORA im Offshore-Windpark Borkum Riffgrund 01" ["Offshore measurement campaign 3 (OMK3) for the project BORA at the offshore-offshore-wind

farm Borkum Riffgrund 01"], Version 2, Project Number: 2271-14-bel (ITAP, Wein, Austria).
ITAP (**2015b**). "Offshore Messkampagne 2 (OMK 2) für das Projekt BORA im Offshore-Windpark Global Tech I" ["Offshore measurement campaign 2 (OMK2) for the project BORA at the offshore-offshore-wind farm Global Tech I"], Version 4, Project Number: 2162-13-bel (ITAP, Wein, Austria).
ITAP (**2015c**). "Offshore Wind Farm Eneco Luchterduinen, ecological monitoring of underwater noise during piling at Offshore Wind Farm Eneco Luchterduinen," Version 5, Project Number: 2322-14-bel (ITAP, Wein, Austria).
ITAP (**2015d**). "Offshore Wind Farm Gemini, ecological monitoring of underwater noise during piling at Offshore Wind Farm Gemini," Version 1, Project Number: 2571-15 (ITAP, Wein, Austria).
Kastelein, R. A., Gransier, R., Marijt, M. A., and Hoek, L. (**2015**). "Hearing frequency thresholds of harbor porpoises (*Phocoena phocoena*) temporarily affected by played back offshore pile driving sounds," J. Acoust. Soc. Am. **137**, 556–564.
Kastelein, R. A., Helder-Hoek, L., Covi, J., and Gransier, R. (**2016**). "Pile driving playback sounds and temporary threshold shift in harbor porpoises (*Phocoena phocoena*): Effect of exposure duration," J. Acoust. Soc. Am. **139**, 2842–2851.
Kastelein, R. A., Helder-Hoek, L., Kommeren, A., Covi, J., and Gransier, R. (**2018**). "Effect of pile-driving sounds on harbor seal (*Phoca vitulina*) hearing," J. Acoust. Soc. Am. **143**, 3583–3594.
Kastelein, R. A., Helder-Hoek, L., Van de Voorde, S., von Benda-Beckmann, A. M., Lam, F. P. A., Jansen, E., de Jong, C. A. F., and Ainslie, M. A. (**2017**). "Temporary hearing threshold shift in a harbor porpoise (*Phocoena phocoena*) after exposure to multiple airgun sounds," J. Acoust. Soc. Am. **142**, 2430–2442.
Lippert, S., Nijhof, M., Lippert, T., Wilkes, D., Gavrilov, A., Heitmann, K., and Ehrlich, J. (**2016**). "COMPILE—A generic benchmark case for predictions of marine pile-driving noise," IEEE J. Oceanic Engineering **41**(4), 1061–1071.
Lippert, T., Ainslie, M. A., and von Estorff, O. (**2018**). "Pile driving acoustics made simple: Damped cylindrical spreading model," J. Acoust. Soc. Am. **143**, 310–317.
Lippert, T., Galindo-Romero, M., Gavrilov, A. N., and von Estorff, O. (**2015**). "Empirical estimation of peak pressure level from sound exposure level. Part II: Offshore impact pile driving noise," J. Acoust. Soc. Am. **138**, EL287–EL292.
Liu, H., Zhang, J., Guo, P., Bi, F., Yu, H., and Ni, G. (**2015**). "Sound quality prediction for engine-radiated noise," Mech. Syst. Signal Process. **56–57**, 277–287.
Lucke, K., Siebert, U., Lepper, P. A., and Blanchet, M. A. (**2009**). "Temporary shift in masked hearing thresholds in a harbor porpoise (*Phocoena phocoena*) after exposure to seismic airgun stimuli," J. Acoust. Soc. Am. **125**, 4060–4070.
Martin, S. B., and Barclay, D. R. (**2019**). "Determining the dependence of marine pile driving sound levels on strike energy, pile penetration, and propagation effects using a linear mixed model based on damped cylindrical spreading," J. Acoust. Soc. Am. **146**(1), 109–121.
Moors, J. J. A. (**1986**). "The meaning of kurtosis: Darlington reexamined," Am. Stat. **40**(4), 283.
Müller, R. A. J., von Benda-Beckmann, A. M., Halvorsen, M. B., and Ainslie, M. A. (**2020**). "Application of kurtosis to underwater sound," J. Acoust. Soc. Am. (in press).
NMFS (**2018**). "2018 Revisions to: Technical guidance for assessing the effects of anthropogenic sound on marine mammal hearing (version 2.0): Underwater thresholds for onset of permanent and temporary threshold shifts," NOAA Technical Memorandum NMFS-OPR-59, U.S. Department of Commerce, National Oceanic and Atmospheric Administration, https://www.fisheries.noaa.gov/resource/document/technical-guidance-assessing-effects-anthropogenic-sound-marine-mammal (Last viewed August 28, 2018).
Popper, A. N., Hawkins, A. D., Fay, R. R., Mann, D. A., Bartol, S., Carlson, T. J., Coombs, S., Ellison, W. T., Gentry, R. L., Halvorsen, M. B., Løkkeborg, S., Rogers, P. H., Southall, B. L., Zeddies, D. G., and Tavolga, W. N. (**2014**). *Sound Exposure Guidelines for Fishes and Sea Turtles: A Technical Report Prepared by ANSI-Accredited Standards Committee S3/SC1 and Registered with ANSI, ASA S3/SC1. 4 TR-2014* (Springer, Heidelberg).
Reinhall, P. G., and Dahl, P. H. (**2011**). "Underwater Mach wave radiation from impact pile driving: Theory and observation," J. Acoust. Soc. Am. **130**, 1209–1216.
Scholik-Schlomer, A. (**2015**). "Where the decibels hit the water: Perspectives on the application of science to real-world underwater noise and marine protected species issues," Acoust. Today **11**(3), 36–44.
Southall, B. L., Bowles, A. E., Ellison, W. T., Finneran, J. J., Gentry, R. L., Greene, C. R., Jr., Kastak, D., Ketten, D. R., Miller, J. H., Nachtigall, P. E., Richardson, W. J., Thomas, J. A., and Tyack, P. L. (**2007**). "Marine mammal noise exposure criteria: Initial scientific recommendations," Aquat. Mam. **33**(4), 1–121.
Southall, B. L., Finneran, J. J., Reichmuth, C., Nachtigall, P. E., Ketten, D. R., Bowles, A. E., Ellison, W. T., Nowacek, D. P., and Tyack, P. L. (**2019**). "Marine mammal noise exposure criteria: Updated scientific recommendations for residual hearing effects," Aquat. Mam. **45**(2), 125–232.
Tougaard, J., Carstensen, J., Teilmann, J., Skov, H., and Rasmussen, P. (**2009**). "Pile driving zone of responsiveness extends beyond 20 km for harbor porpoises (*Phocoena phocoena* (L.))," J. Acoust. Soc. Am. **126**, 11–14.
Zampolli, M., Nijhof, M. J. J., de Jong, C. A. F., Ainslie, M. A., Jansen, E. H., and Quesson, B. A. J. (**2013**). "Validation of finite element computations for the quantitative prediction of underwater noise from impact pile driving," J. Acoust. Soc. Am. **133**, 72–81.